Exponential Bhatnagar-Gross-Krook integrator for multiscale particle-based kinetic simulations

M. Pfeiffer [*] and F. Garmirian [†]
Institute of Space Systems, University of Stuttgart, Pfaffenwaldring 29, 70569 Stuttgart, Germany

M. H. Gorji [‡]
Laboratory of Multiscale Studies in Building Physics, Empa, Swiss Federal Laboratories for Materials Science and Technology, Dübendorf, Switzerland

(Received 15 February 2022; revised 15 July 2022; accepted 20 July 2022; published 4 August 2022)

Despite the development of an extensive toolbox of multiscale rarefied flow simulators, such simulations remain challenging due to the significant disparity of collisional and macroscopic spatiotemporal scales. Our study offers a novel and consistent numerical scheme for a coupled treatment of particles advection and collision governed by the BGK evolution, honoring positivity of the velocity distribution. Our method shares its framework, in spirit, with the unified gas kinetic class of multiscale schemes. Yet it provides attractive features for particle-based stochastic simulations, readily implementable to existing direct simulation Monte Carlo codes. Two main innovations are integrated in the presented BGK particle method. The first ingredient is a high-order time integration that can be interpreted probabilistically, independent of the time step size. The next one is identifying modified particle distributions that remain invariant under the advection-relaxation evolution. We demonstrate accuracy and performance of the devised scheme for prototypic gas flows over a wide range of rarefaction parameters. Due to the resulting robustness and flexibility of the devised exponential BGK integrator, the scheme paves the way towards more affordable simulations of large-scale and multiscale rarefied gas phenomena.

DOI: 10.1103/PhysRevE.106.025303

I. INTRODUCTION

The direct simulation Monte Carlo (DSMC) method has become the standard approach for simulations of rarefied nonequilibrium gas flows [1]. It is built on the main idea of employing discrete particle collisions in order to statistically mimic the molecular collisions. An important success element of DSMC rests on the particle-based treatment of the phase space, which allows rather straightforward integration of the inner energy modes and chemical reactions, as well as boundary interactions. Despite the established accuracy of DSMC across the whole rarefaction regimes, it comes with a drawback of dense operations near the continuum because the mean-free path and the collision frequency have to be resolved. As a consequence, it is still challenging to simulate flows with large variation of the Knudsen number, covering both continuum and rarefied phenomena. To overcome this central issue, different approaches have been proposed. The most direct solution is to couple continuum solvers based on the Navier-Stokes equations with DSMC [2,3]. However, since the two solvers operate at different levels of the flow description, i.e., macroscopic variables in the Navier-Stokes and particle-based probabilities in DSMC, various problems arise which limit the generality and robustness of such approaches.

Another possibility is offered by multiscale methods based on the discretization of the phase space, as provided e.g., in discrete-velocity methods (DVMs) [4]. Along DVMs, recently there have been several developments such as UGKS [5,6] and DUKGS [7], where Bhatnagar-Gross-Krook (BGK) approximations of the collision term are computed efficiently. Due to the deterministic treatment of the kinetic problem, these methods provide noise-free solutions, which make them well suited for low-Mach flows. However, this comes with the price of the velocity-space discretization, which might render these methods inefficient for high-Mach nonequilibrium flows with significantly extended velocity domains.

An interesting remedy to circumvent this problem is provided by the UGKWP method [8]. Here the nonequilibrium part of the velocity distribution is represented by particles, to reduce the corresponding cost of the velocity discretization. Furthermore, such hybrid representation allows for noise-free solutions in the hydrodynamic limit, as particles are employed only in the nonequilibrium portions of the flow. Nevertheless, a mixed-particle-DVM treatment of the distribution leads to implementation challenges, especially if the approach is to be integrated into the existing mature DSMC solvers.

On a different front, quite a few particle-based BGK [9–11] and Fokker-Planck (FP) [12–14] methods have come to the fore in recent years, as they could simply be coupled with DSMC while also being efficient at moderate and low Knudsen flows. On the BGK side, especially the particle-based ellipsoidal statistical BGK [15,16] (ES-BGK) and the Shakhov BGK methods were investigated [9,17]. For the FP

[*]Corresponding author: mpfeiffer@irs.uni-stuttgart.de
[†]garmirianf@irs.uni-stuttgart.de
[‡]Mohammadhossein.Gorji@empa.ch

models, the main work was done on the entropic FP model (EFP) [13], cubic-FP model [18], ellipsoidal statistical FP (ESFP) model [14], and Bogomolov's model [19]. However, while the proposed schemes might reduce the cost of dense collisions in the continuum regime, they still need fine resolutions. This is due to the typical first-order treatment of particles' evolution, which is implied by splitting between free flight and collision-relaxation subtime steps.

In this study, we devise a particle-based multiscale BGK solver. We remain in the realm of pure particle representation of the distribution with identical positive statistical weights. This avoids implementation overheads of integrating the scheme with existing DSMC solvers. Moreover, we anticipate straightforward extensions to more complex nonequilibrium phenomena (e.g., chemical reactions). The multiscale capability of the scheme is achieved by coupled position-velocity integration of the particles evolution. After applying a high-order time integration scheme, we identify modified distributions that remain invariant under advection-relaxation steps. This relaxes the assumption of frozen target distribution per time step, commonly made for BGK particle methods. Furthermore, by employing exponential time integrators, the scheme ensures that the particles are sampled from well-defined distributions independent of the time step size. In the following, we discuss the details of the scheme after a brief review of the governing theory.

II. THEORY

The Boltzmann equation describes a monatomic gas flow with the corresponding distribution function $f = f(\mathbf{x}, \mathbf{v}, t)$ at position $\mathbf{x}$ and velocity $\mathbf{v}$,

$$\frac{\partial f}{\partial t} + \mathbf{v} \cdot \frac{\partial f}{\partial \mathbf{x}} = \left.\frac{\delta f}{\delta t}\right|_{\text{coll}}, \tag{1}$$

where external forces are neglected and $\delta f/\delta t|_{\text{coll}}$ follows the Boltzmann collision integral

$$\left.\frac{\partial f}{\partial t}\right|_{\text{coll}} = \int_{\mathbb{R}^3}\int_{S^2} B[f(\mathbf{v}')f(\mathbf{v}'_*) - f(\mathbf{v})f(\mathbf{v}_*)]\, d\mathbf{n}\, d\mathbf{v}_*. \tag{2}$$

Here $S^2 \subset \mathbb{R}^3$ is the unit sphere, $\mathbf{n}$ is the unit vector of the scattered velocities, B is the collision kernel, and the prime superscript denotes postcollision velocities. The multiple integration of this nonlinear collision term, besides high dimensionality of the solution domain, makes the Boltzmann collision integral computationally complex. For this reason, the DSMC method reduces the collision integral to the Monte Carlo sampling of collision events among random particles representing the gas flow. Either through direct solvers or by random particles, the mean-free path as well as the collision frequency must be resolved, leading to a significant computational effort for low Knudsen number flows.

A. BGK approximation

The BGK model approximates the collision term by a nonlinear relaxation form, where the distribution f relaxes towards a target f^t,

$$\left.\frac{\partial f}{\partial t}\right|_{\text{Coll}} = \Omega = \nu(f^t - f), \tag{3}$$

with a certain relaxation frequency ν. It is assumed, in the original BGK model, that the target distribution is the Maxwellian

$$f^M = n\Big(\frac{m}{2\pi k_B T}\Big)^{3/2} \exp\Big[-\frac{m\mathbf{c}\cdot\mathbf{c}}{2k_B T}\Big], \tag{4}$$

with the number density n, molecular mass m, temperature T, Boltzmann constant k_B, and thermal velocity $\mathbf{c} = \mathbf{v} - \mathbf{u}$ with the average flow velocity $\mathbf{u}$ [20]. The relaxation frequency gives rise to the viscosity

$$\mu = \frac{nk_B T}{\nu}. \tag{5}$$

The Maxwellian distribution, as the target, leads to the fixed Prandtl number of $\text{Pr} = \mu c_P/K = 1$, whereas the Prandtl number for monatomic gases is close to $2/3$ [21]. To overcome this problem, several extensions of the BGK model have been introduced. Some of these models transform the target distribution function, e.g., the ellipsoidal statistical BGK model [22] or the Shakhov BGK model [23], while others modify the relaxation frequency from a constant to a function of the microscopic velocities as described by Struchtrup [24].

B. Particle-based BGK solver

While the BGK relaxation has a much simpler construct compared to the Boltzmann collision integral, still stiff relaxation might be encountered if explicit time integrations are applied. Furthermore, to obtain asymptotical convergence to the Navier-Stokes equations, the advection (particle movement) and the relaxation term should be treated in a coupled way, as discussed in Refs. [5,7].

In the stochastic particle BGK method (SP-BGK), the time integration of Eq. (3) is typically done by assuming a constant target distribution [15,16]:

$$f(\mathbf{v}, \mathbf{x}, t + \Delta t) = e^{-\nu\Delta t} f(\mathbf{v}, \mathbf{x}, t) + (1 - e^{-\nu\Delta t}) f^t(\mathbf{v}, \mathbf{x}, t). \tag{6}$$

The advection part follows a first-order operator splitting, which means that the particles of $f(\mathbf{v}, \mathbf{x}, t + \Delta t)$ are moved along their trajectory for a full time step Δt to reach $f(\mathbf{v}, \mathbf{x} + \mathbf{v}\Delta t, t + \Delta t)$. This first-order time integration has some advantages for particle methods. For $\nu\Delta t \ll 1$, the time integration (6) recovers the forward Euler method

$$f(\mathbf{v}, \mathbf{x}, t + \Delta t) = (1 - \nu\Delta t) f(\mathbf{v}, \mathbf{x}, t) + \nu\Delta t f^t(\mathbf{v}, \mathbf{x}, t). \tag{7}$$

Yet in contrast to the forward Euler equation (7), the prefactors of $f(\mathbf{v}, \mathbf{x}, t)$ and f^t are always positive in Eq. (6), also when $\nu\Delta t > 1$. In the stochastic particle method context, Eq. (6) can be easily realized if each particle within a cell gets a new velocity sampled from f^t with the well-posed probability $(1 - e^{-\nu\Delta t})$. For the Euler forward method, however, similar realizations work only as long as $\nu\Delta t$ remains below 1. Otherwise, particles with negative weights have to be introduced in order to construct the desired distribution function, as the prefactor of $f(\mathbf{v}, \mathbf{x}, t)$ becomes negative in Eq. (7). While $\nu\Delta t > 1$ may not be relevant for the first-order explicit time integration, the unconditional positivity of the distribution function reveals the advantage of Eq. (6) over Eq. (7) for particle methods, in terms of both the robustness as well as the implementation.

To improve the explicit time integration to a second-order method coupling advection and relaxation, we follow UGKS [5,6] and DUGKS [7]. The Crank-Nicolson method is used for the time integration

$$f(\mathbf{v}, \mathbf{x} + \mathbf{v}\Delta t, t + \Delta t) = f(\mathbf{v}, \mathbf{x}, t) + \frac{\Delta t}{2}[\Omega(\mathbf{v}, \mathbf{x} + \mathbf{v}\Delta t, t + \Delta t) + \Omega(\mathbf{v}, \mathbf{x}, t)]. \tag{8}$$

Next, let us introduce two additional distributions

$$\tilde{f} = f - \frac{\Delta t}{2}\Omega = \frac{2\tau + \Delta t}{2\tau} f - \frac{\Delta t}{2\tau} f^t \tag{9}$$

$$\text{and} \quad \hat{f} = f + \frac{\Delta t}{2}\Omega = \frac{2\tau - \Delta t}{2\tau} f + \frac{\Delta t}{2\tau} f^t, \tag{10}$$

with $\tau = 1/\nu$ being the relaxation time. After inserting the above-introduced distributions into Eq. (8), one sees that $\tilde{f}(\mathbf{v}, \mathbf{x} + \mathbf{v}\Delta t, t + \Delta t)$ is nothing but the particles of $\hat{f}(\mathbf{v}, \mathbf{x}, t)$, which are moved along their trajectories for Δt,

$$\tilde{f}(\mathbf{v}, \mathbf{x} + \mathbf{v}\Delta t, t + \Delta t) = \hat{f}(\mathbf{v}, \mathbf{x}, t). \tag{11}$$

This approach provides an implicit integration of the coupled advection and relaxation, suitable in theory also for stochastic particle methods. Note that, in the case of DVM (including UGKS and DUGKS), some additional work has to be done for the flux reconstruction.

Nevertheless, for stochastic particle methods the problem of negative prefactors for large Δt arises again, so that additional particles with partly negative weighting factors would have to be added to construct the distribution functions. A practical solution was provided by Fei *et al.* [25,26], where an additional collision term was inserted in which the current distribution function is approximated by a Grad-13 approximation. This allows the advection and the relaxation process to be solved together. The choice of the Grad-13 distribution also ensures that the Navier-Stokes limit is asymptotically preserved. This additional collision term is constructed to satisfy the Navier-Stokes equations in the continuum domain with a second-order time integration, whereas a conventional first-order SP-BGK method is applied in the rarefied domain. Finally, a multiscale parameter was defined, allowing a smooth transition between the normal SP-BGK method and the one subject to the Grad-13 approximation. Nevertheless, in the transition regime and depending on the choice of the multiscale parameter, either the entire method falls back to SP-BGK and is therefore first order, or one gets a mixture of the SP-BGK method and the additional collision term, whose order should then also fall back to the first order, and the error due to the interpolation between the normal SP-BGK method and the additional collision term is not quite clear.

Even though a good performance of the SP-BGK method regularized by Grad-13 approximation has been demonstrated, it is still desirable to construct a rigorous SP-BGK algorithm with overarching properties of the DSMC method, without the need of introducing auxiliary approximations to deal with the negative prefactors. In the following, we construct such a second-order particle method without making additional approximations on the distribution functions. Thus, the introduction of an additional multiscale parameter is omitted, and the construction would become consistent with the BGK equation, in a fashion similar to UGKS and DUGKS.

C. Exponential time differencing of the BGK equation

The exponential time differencing has advantages especially in dealing with ordinary differential equations that contain a stiff linear term [27]

$$\dot{u} = cu + F(u, t), \tag{12}$$

where c is a constant that leads to the stiff system, and F is the nonlinear part. The main idea is to integrate the stiff term in the exact form, and then approximate the nonlinear term numerically (typically explicitly) as

$$u(t + \Delta t) = u(t)e^{c\Delta t} + e^{c\Delta t}\int_0^{\Delta t} e^{-cs} F(u(t + s), t + s)\, ds, \tag{13}$$

which is exact up to the point where the occurring integral is approximated. If we now look at the relaxation term of the BGK equation in a form corresponding to Eq. (12),

$$\partial f/\partial t = -\nu f + \nu f^t, \tag{14}$$

we face an additional problem that the nonlinear part νf^t is also stiff (since it scales with ν). Following Eq. (13), we get

$$f(t + \Delta t) = f(t)e^{-\nu\Delta t} + e^{-\nu\Delta t}\int_0^{\Delta t} e^{\nu s}\nu f^t(t + s)\, ds. \tag{15}$$

Now, in order to treat the stiffness of the nonlinear term, an implicit integration, such as the Crank-Nicolson method similar to the DUGKS method, can be carried out. In the following, we carry out this procedure, and it is shown that it has various advantages for particle methods, since the prefactors mentioned always remain positive.

1. Linear approximation

Let f^t_{t+s} and f^t_t represent the numerical approximations of the target distribution at time steps $t + s$ and t, respectively. To construct a second-order scheme, we adopt the following linear approximation for the target distribution:

$$f^t_{t+s} = f^t_t + \frac{s}{\Delta t}\left(f^t_{t+\Delta t} - f^t_t\right) \tag{16}$$

leading to a Crank-Nicolson-type scheme. Using this approximation, the integration of Eq. (15) yields to

$$f_{t+\Delta t} = f_t e^{-\nu\Delta t} + e^{-\nu\Delta t}\left[f^t_t\left(\frac{e^{\nu\Delta t}}{\nu\Delta t} - 1 - \frac{1}{\nu\Delta t}\right) + f^t_{t+\Delta t}\left(e^{\nu\Delta t} + \frac{1}{\nu\Delta t} - \frac{e^{\nu\Delta t}}{\nu\Delta t}\right)\right], \tag{17}$$

where $f_{t+\Delta t}$ and f_t denote the numerical approximations of $f(t + \Delta t)$ and $f(t)$, respectively. After a few rearrangements and taking particle movement into account, Eq. (17) leads to the following integration scheme:

$$f_{t+\Delta t}(\mathbf{v}, \mathbf{x} + \mathbf{v}\Delta t) = f_t(\mathbf{v}, \mathbf{x})e^{-\nu\Delta t} + (1 - e^{-\nu\Delta t}) \times \left[A f^t_t(\mathbf{v}, \mathbf{x}) + B f^t_{t+\Delta t}(\mathbf{v}, \mathbf{x} + \mathbf{v}\Delta t)\right], \tag{18}$$

with

$$A = \frac{1}{\nu\Delta t} - \frac{e^{-\nu\Delta t}}{1-e^{-\nu\Delta t}} \tag{19}$$

$$\text{and} \quad B = \frac{1}{1-e^{-\nu\Delta t}} - \frac{1}{\nu\Delta t}. \tag{20}$$

Equation (18) already contains the simple form of the first-order SP-BGK method (6). Furthermore the prefactors $A \in [0, 0.5]$ and $B \in [0.5, 1]$ are nonnegative. Following Refs. [5,7], two additional distributions can be introduced:

$$\hat{f} = f_t e^{-\nu\Delta t} + (1-e^{-\nu\Delta t})A f_t^t \tag{21}$$

$$\text{and} \quad \tilde{f} = f_t - (1-e^{-\nu\Delta t})B f_t^t, \tag{22}$$

whereby once more

$$\tilde{f}(\mathbf{v}, \mathbf{x}+\mathbf{v}\Delta t, t+\Delta t) = \hat{f}(\mathbf{v}, \mathbf{x}, t) \tag{23}$$

is honored. Therefore, by moving the particles of $\hat{f}(\mathbf{v}, \mathbf{x}, t)$ along the trajectories $\tilde{f}(\mathbf{v}, \mathbf{x}+\mathbf{v}\Delta t, t+\Delta t)$, the advection and relaxation processes are coupled and the time integration remains second-order accurate. Starting from $f_t(\mathbf{v}, \mathbf{x})$, $\hat{f}(\mathbf{v}, \mathbf{x}, t)$ can be constructed from Eq. (21). Afterwards, $\tilde{f}(\mathbf{v}, \mathbf{x}+\mathbf{v}\Delta t, t+\Delta t)$ is realized by moving the particles from $\hat{f}(\mathbf{v}, \mathbf{x}, t)$, and finally $f_{t+\Delta t}(\mathbf{v}, \mathbf{x}+\mathbf{v}\Delta t)$ is constructed via

$$f_t = \tilde{f} + (1-e^{-\nu\Delta t})B f_t^t. \tag{24}$$

While all prefactors remain nonnegative, a renormalization has to be introduced because the prefactors of Eqs. (21) and (24) do not sum up to unity. To avoid deleting and creating particles, the introduced distribution functions are normalized by the factor

$$\gamma = e^{-\nu\Delta t} + (1-e^{-\nu\Delta t})A = \frac{1-e^{-\nu\Delta t}}{\nu\Delta t}, \tag{25}$$

which results in new distributions $\hat{f}^* = \hat{f}/\gamma$ and $\tilde{f}^* = \tilde{f}/\gamma$, with $\tilde{f}^*(\mathbf{v}, \mathbf{x}+\mathbf{v}\Delta t, t+\Delta t) = \hat{f}^*(\mathbf{v}, \mathbf{x}, t)$, leading to

$$\begin{aligned}\hat{f}^* &= \frac{e^{-\nu\Delta t}}{\gamma} f_t + \frac{1-e^{-\nu\Delta t}}{\gamma} A f_t^t \\ &= \frac{\nu\Delta t e^{-\nu\Delta t}}{1-e^{-\nu\Delta t}} f_t + \left(1 - \frac{\nu\Delta t e^{-\nu\Delta t}}{1-e^{-\nu\Delta t}}\right) f_t^t \end{aligned} \tag{26}$$

$$\begin{aligned}\text{and} \quad f_t &= \gamma\tilde{f}^* + (1-e^{-\nu\Delta t})B f_t^t \\ &= \frac{1-e^{-\nu\Delta t}}{\nu\Delta t}\tilde{f}^* + \left(1 - \frac{1-e^{-\nu\Delta t}}{\nu\Delta t}\right) f_t^t. \end{aligned} \tag{27}$$

To further simplify the time integration, one can also omit the intermediate step via f and track only the additional distribution functions $\tilde{f}^*$ and $\hat{f}^*$. By substituting Eq. (26) into (27), we get

$$\hat{f}^* = e^{-\nu\Delta t}\tilde{f}^* + (1-e^{-\nu\Delta t}) \underbrace{\left[\frac{B e^{-\nu\Delta t}}{\gamma} + \frac{A}{\gamma}\right]}_{=1} f_t^t. \tag{28}$$

This is a convenient formulation as similar to the original SP-BGK, particles have to be sampled from the target distribution with the probability $(1-e^{-\nu\Delta t})$ to construct $\hat{f}^*$ from $\tilde{f}^*$. The two most common target distributions are the ellipsoidal statistical BGK (ES-BGK) and the Shakhov model (S-BGK). The ES-BGK distribution is given as

$$f^{ES} = \frac{n}{\sqrt{\det(2\pi\lambda_{ij})}} \exp\left[-\frac{1}{2}\lambda_{ij}^{-1} c_i c_j\right] \tag{29}$$

with the matrix

$$\lambda_{ij} = \frac{k_B T}{m}\delta_{ij} + \left(1 - \frac{1}{\mathrm{Pr}}\right)\frac{p_{\langle ij\rangle}}{\rho}. \tag{30}$$

Here δ_{ij} is the Kronecker delta, Pr is the Prandtl number, ρ is the mass density, and $p_{\langle ij\rangle}$ is the traceless pressure tensor

$$p_{\langle ij\rangle} = m\int c_{\langle i} c_{j\rangle} f \, d\mathbf{c}. \tag{31}$$

In the case of the S-BGK model, the target distribution is defined as

$$f^S = f^M\left[1 + (1-\mathrm{Pr})\frac{\mathbf{c}\cdot\mathbf{q}}{5\rho(RT)^2}\left(\frac{\mathbf{c}\cdot\mathbf{c}}{2RT} - \frac{5}{2}\right)\right] \tag{32}$$

with the heat flux vector

$$\mathbf{q} = \frac{1}{2}m\int \mathbf{c}(\mathbf{c}\cdot\mathbf{c}) f \, d\mathbf{c}. \tag{33}$$

Therefore to evaluate Eq. (28), knowledge about either $p_{\langle ij\rangle}(f)$ or $\mathbf{q}(f)$ becomes necessary. Due to the normalization of the distributions, as already extensively discussed in Refs. [5,7], the mass, momentum, and energy are conserved by the collision operator and thus can be determined directly from the additional distributions

$$\rho = \int m f \, d\mathbf{v} = \int m\hat{f}^* \, d\mathbf{v} = \int m\tilde{f}^* \, d\mathbf{v}, \tag{34}$$

$$\rho\mathbf{u} = \int m\mathbf{v} f \, d\mathbf{v} = \int m\mathbf{v}\hat{f}^* \, d\mathbf{v} = \int m\mathbf{v}\tilde{f}^* \, d\mathbf{v}, \tag{35}$$

$$\begin{aligned}\text{and } \rho\epsilon &= \frac{3}{2}nk_B T \\ &= \int \frac{m}{2}\mathbf{c}^2 f \, d\mathbf{v} = \int \frac{m}{2}\mathbf{c}^2\hat{f}^* \, d\mathbf{v} = \int \frac{m}{2}\mathbf{c}^2\tilde{f}^* \, d\mathbf{v} \end{aligned} \tag{36}$$

with $\rho\epsilon$ being the internal energy. Neither $p_{\langle ij\rangle}(f)$ nor $\mathbf{q}(f)$ would be preserved during the relaxation process, yet can be calculated directly from $\tilde{f}^*$:

$$p_{\langle ij\rangle}(f_t) = \frac{1-e^{-\nu\Delta t}}{\nu\Delta t} p_{\langle ij\rangle}(\tilde{f}^*) \tag{37}$$

$$\text{and} \quad \mathbf{q}(f_t) = \frac{1-e^{-\nu\Delta t\mathrm{Pr}}}{\nu\Delta t\mathrm{Pr}}\mathbf{q}(\tilde{f}^*). \tag{38}$$

Following the ES-BGK target distribution, we can summarize the algorithmic steps of the devised second-order time integration, whose computational complexity is almost identical to the first-order conventional SP-BGK methods:

(1) Initialize the particles in the simulation domain (similar to DSMC) method to obtain f_t.

(2) Use Eq. (26) to construct $\hat{f}^*$ from f_t by sampling the particles from f_t^t with the probability $1 - \nu\Delta t e^{-\nu\Delta t}/(1-e^{-\nu\Delta t})$.

(3) Move the particles of $\hat{f}^*$ in the physical domain (and apply the boundary conditions similar to DSMC) to construct $\tilde{f}^*(\mathbf{v}, \mathbf{x}+\mathbf{v}\Delta t, t+\Delta t) = \hat{f}^*(\mathbf{v}, \mathbf{x}, t)$.

(4) Construct $\hat{f}^*(\mathbf{v}, \mathbf{x}+\mathbf{v}\Delta t, t+\Delta t)$ out of $\tilde{f}^*(\mathbf{v}, \mathbf{x}+\mathbf{v}\Delta t, t+\Delta t)$ using Eq. (28), by sampling the particles from f_t^t with the probability $(1-e^{-\nu\Delta t})$ given the pressure tensor and heat fluxes from Eqs. (37) and (38).

(5) Repeat steps 3 and 4 for the entire duration of the simulation.

2. Exponential approximation

The devised scheme can be further improved by applying exponential relaxation

$$f_{t+s}^t = f_t^t + \frac{1-e^{-\nu s}}{1-e^{-\nu\Delta t}}\left(f_{t+\Delta t}^t - f_t^t\right) \tag{39}$$

instead of the linear approximation of Eq. (16). The two additional distributions are then modified with the prefactors

$$A^{(\mathrm{exp})} = 1 - \frac{1}{1-e^{-\nu\Delta t}} + \frac{\nu\Delta t e^{-\nu\Delta t}}{(1-e^{-\nu\Delta t})^2} \tag{40}$$

$$B^{(\mathrm{exp})} = \frac{1}{1-e^{-\nu\Delta t}} - \frac{\nu\Delta t e^{-\nu\Delta t}}{(1-e^{-\nu\Delta t})^2} \tag{41}$$

resulting in a modified $\gamma^{(\mathrm{exp})}$ for the normalization

$$\gamma^{(\mathrm{exp})} = e^{-\nu\Delta t} + (1-e^{-\nu\Delta t})A^{(\mathrm{exp})} = \frac{\nu\Delta t e^{-\nu\Delta t}}{1-e^{-\nu\Delta t}}. \tag{42}$$

Thus the normalized additional distributions for the exponential approximation are given as

$$\hat{f}^{*,(\mathrm{exp})} = \frac{1-e^{-\nu\Delta t}}{\nu\Delta t} f + \left(1 - \frac{1-e^{-\nu\Delta t}}{\nu\Delta t}\right) f_t^t \tag{43}$$

$$\text{and} \quad f_t = \frac{\nu\Delta t e^{-\nu\Delta t}}{1-e^{-\nu\Delta t}} \tilde{f}^{*,(\mathrm{exp})} + \left(1 - \frac{\nu\Delta t e^{-\nu\Delta t}}{1-e^{-\nu\Delta t}}\right) f_t^t. \tag{44}$$

Interestingly, this exponential approximation just swaps the prefactors in Eqs. (43) and (44) compared to Eqs. (26) and (27) of the linear approach. Therefore, this results again in

$$\hat{f}^{*,(\mathrm{exp})} = e^{-\nu\Delta t}\tilde{f}^{*,(\mathrm{exp})} + (1-e^{-\nu\Delta t}) f_t^t. \tag{45}$$

The only difference that arises is the calculation of the pressure tensor and the heat flux from $\tilde{f}^{*,(\mathrm{exp})}$:

$$p_{\langle ij\rangle}(f_t) = \frac{\nu\Delta t e^{-\nu\Delta t}}{1-e^{-\nu\Delta t}} p_{\langle ij\rangle}(\tilde{f}^{*,(\mathrm{exp})}) \tag{46}$$

$$\text{and} \quad \mathbf{q}(f_t) = \nu\Delta t \mathrm{Pr}\, \frac{e^{-\nu\Delta t Pr}}{1-e^{-\nu\Delta t Pr}} \mathbf{q}(\tilde{f}^{*,(\mathrm{exp})}). \tag{47}$$

3. Properties of the ED-BGK method

The behavior of the introduced particle scheme with exponential differencing (ED-BGK) is analyzed in the limits of free-molecular and continuum regimes. In the following and without loss of generality, the discussion is limited to the linear approximation. In the free molecular regime ($\tau \gg \Delta t$), Eqs. (26) and (27) simplify to

$$\hat{f}^* = f_t, \quad f_t = \tilde{f}^*, \tag{48}$$

which is consistent with the collisionless limit implying $f(\mathbf{v}, \mathbf{x}+\mathbf{v}\Delta t, t+\Delta t) = f(\mathbf{v}, \mathbf{x}, t)$. On the other hand, for the continuum limit ($\tau \ll \Delta t$), the distribution relaxes after a time step Δt based on Eqs. (26) and (27) gives (shown in the Appendix)

$$f\ (\mathbf{v}, \mathbf{x}+\mathbf{v}\Delta t, t+\Delta t) \approx f^M(\mathbf{v}, \mathbf{x}, t) \tag{49}$$

$$-\tau(\partial_t + \mathbf{v}\nabla) f^M(\mathbf{v}, \mathbf{x}, t) + \Delta t \partial_t f^M(\mathbf{v}, \mathbf{x}, t), \tag{50}$$

which recovers the Chapman-Enskog approximation of the Navier-Stokes solution as discussed by Guo *et al.* [7].

III. IMPLEMENTATION

The presented BGK particle method is implemented in the PIC-DSMC code PICLas [28,29] as described in detail by Pfeiffer [9]. The main concept of the particle BGK method, especially the energy and momentum conservation, is based on the works of Gallis and Torczynski [15,16]. The particles are moved in the physical space sorted in a computational mesh, collide with boundaries, and their macroscopic properties are sampled, all similar to DSMC. However, in contrast to the DSMC method, the collision step is replaced by a jump relaxation with the probability

$$P = 1 - \exp[-\nu\Delta t], \tag{51}$$

according to Eq. (28), towards the target distribution. $\hat{f}^*$ is constructed out of f using Eq. (26) or (43) for the linear or the exponential approximation, respectively. Next, $\tilde{f}^*$ is constructed by moving the particles from $\hat{f}^*$ in the next time steps. The difference to the common SP-BGK method is that the pressure tensor or heat flux vector must be relaxed according to Eqs. (37) and (38) or Eqs. (46) and (47) depending whether the linear or the exponential approximation is used before sampling from the target distribution, since these are from f and not from $\tilde{f}^*$. For the ellipsoidal statistical target distribution, only the pressure tensor, and for the Shakhov target distribution, only the heat flux vector is necessary.

To determine the correct relaxation frequency ν, the well-known temperature dependency of the viscosity μ,

$$\mu = \mu_{\mathrm{ref}}\left(\frac{T}{T_{\mathrm{ref}}}\right)^{\omega_{VHS}}, \tag{52}$$

is used, with the reference temperature T_{ref}, and μ_{ref} the reference dynamic viscosity at T_{ref} [30], and ω_{VHS} as the parameter of the variable hard sphere (VHS) model. For a VHS gas, the reference dynamic viscosity can be calculated with the VHS reference diameter d_{ref} of the particles:

$$\mu_{\mathrm{ref}} = \frac{30\sqrt{m k_B T_{\mathrm{ref}}}}{\sqrt{\pi}4(5-2\omega_{VHS})(7-2\omega_{VHS})d_{\mathrm{ref}}^2}. \tag{53}$$

The sampling process itself as well as a detailed discussion of the possible energy and momentum conservation schemes for the particle BGK method can be found in Pfeiffer [9]. For momentum and energy conservation, the final velocities of the particles are corrected according to

$$\mathbf{v}_i^* = \mathbf{u} + \alpha(\mathbf{v}_i' - \mathbf{u}'), \tag{54}$$

where $\mathbf{u} = \sum_{i=1}^N \mathbf{v}_i/N$ is the bulk flow velocity before the relaxation, $\mathbf{v}_i'$ is the particle velocity after the relaxation (uncorrected), and $\mathbf{u}' = \sum_{i=1}^N \mathbf{v}_i'/N$. Note that $\mathbf{v}_i' = \mathbf{v}_i$, if no

relaxation occurs for particle i. Due to

$$\sum_{i=1}^{N}(\mathbf{v}_i' - \mathbf{u}') = 0, \tag{55}$$

Eq. (54) ensures the momentum conservation. The energy conservation is achieved by choosing α as

$$\alpha = \sqrt{\frac{T}{T'}} \tag{56}$$

with T the temperature before relaxation, and T' after the relaxation process (in the absence of energy correction).

In order to achieve second-order accuracy in space, the values that enter the BGK operator are linearly interpolated, instead of being constant values per computational cell. A more detailed discussion, including an alternative to the linear interpolation, especially for particle methods, can be found in Fei *et al.* [25,26]. In this work, a conventional linear interpolation was used, similar to Particle-In-Cell codes, as have already been described for the PICLas code by Fasoulas *et al.* [29], among others.

A. Homogeneous relaxation

The first test case, similar to Fei *et al.* [25], considers a spatially homogeneous relaxation (in a stationary frame of reference) to examine the accuracy of the time integration scheme. In a single adiabatic cell, argon with the particle density $n = 2.7 \times 10^{25}$ m^{-3} and temperature $T = 273$ K is simulated, subject to the initial condition of the 13-moment Grads distribution [31]

$$f^{\text{Grad}} = f^{M}\left[1 + \frac{m^2 p_{\langle ij\rangle}}{2\rho k_B^2 T^2} c_{\langle i} c_{j\rangle} - \frac{m^2 q_j c_j}{\rho k_B^2 T^2}\left(1 - \frac{m}{5k_B T}\mathbf{c}^2\right)\right]. \tag{57}$$

This allows us to initialize the gas in a nonequilibrium state with stresses and heat fluxes. Each deviatoric entry of the pressure tensor was chosen according to $p_{\langle ij\rangle} = 3nk_BT$, whereas the heat flux is set based on $q_i = n(3k_BT)^{3/2}m^{-1/2}$. Relaxation of the pressure tensor and the heat flux vector is analyzed for different time step sizes. The normal SP-BGK method, the proposed exponential differencing SP-BGK (ED-SP-BGK) with the linear approximation [Eq. (16)], and the exponential approximation [Eq. (39)] are employed. A finely resolved DSMC calculation is deployed as the reference. As shown in Fig. 1, the error in the pressure tensor for the standard SP-BGK is significant, as the target distribution is approximated as a constant per time step. Comparing the results depicted in Fig. 2 and Fig. 3, it can be seen that the relaxation is also correctly reproduced for time steps greater than the collision time by the devised ED-SP-BGK model. In the case of the linear approximation, the error in the relaxation of the pressure tensor is greater than the one resulting from the exponential approximation, while the heat flux is reproduced slightly better with the linear approximation.

B. Sod shock tube

The well-known Sod test case is considered in two different regimes. Argon was again used for the simulations. The physical domain has a length of 1 m. The starting temperature in the entire simulation domain is 273 K. However, the particle density differs in the left n_l, $x \in [0, 0.5]$ and the right n_r, $x \in [0.5, 1]$ subdomains. For the rarefied case, the densities $n_l = 1.508 \times 10^{19}$ m^{-3} and $n_r = 1.885 \times 10^{18}$ m^{-3} were chosen. This results in a Knudsen number of about Kn ≈ 0.1. In the continuum case, the imposed densities are $n_l = 1.508 \times 10^{21}$ m^{-3} and $n_r = 1.885 \times 10^{20}$ m^{-3} resulting in a Knudsen number Kn ≈ 0.001. The reference solutions were generated with DSMC.

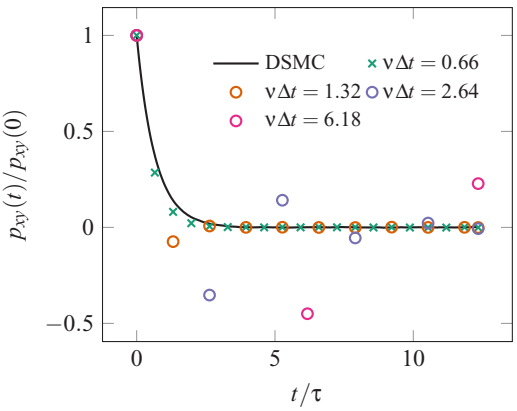

(a) Normalized shear stress

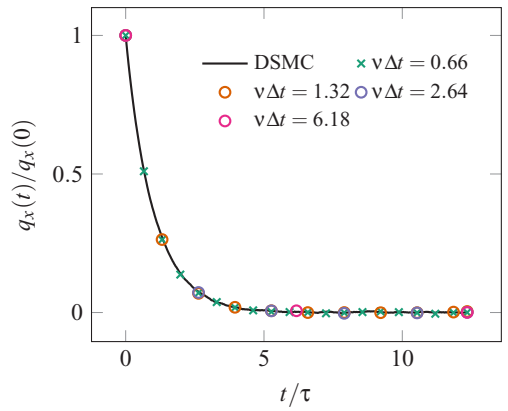

(b) Normalized heat flux

FIG. 1. Pressure tensor and heat flux relaxations with different time step sizes Δt using SP-BGK method. The finely resolved DSMC results are provided as the reference. The time is normalized using the relaxation time τ.

In the rarefied case, a computational mesh with 60 grid cells was used for both DSMC and ED-SP-BGK simulations. Also the time step $\Delta t = 3 \times 10^{-5}$ s was the same for both methods, resulting in $\nu\Delta t \approx 0.035$ for the ED-SP-BGK method. As depicted in Fig. 4, the DSMC result is very well matched with the ED-SP-BGK method. To achieve the same physical time in the rarefied case, DSMC and the EIBGK method require pretty much the same simulation time. This is also understandable since in this case the same time step size and the same number of particles can be used.

In the case of the continuum flow, while spatiotemporal discretization of DSMC was adjusted to resolve the collisional scales, the mesh similar to the rarefied setting was used for

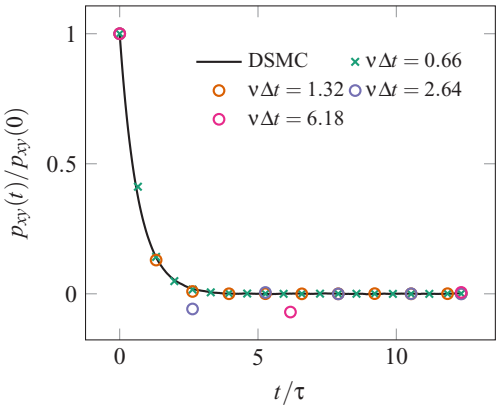

(a) Normalized shear stress

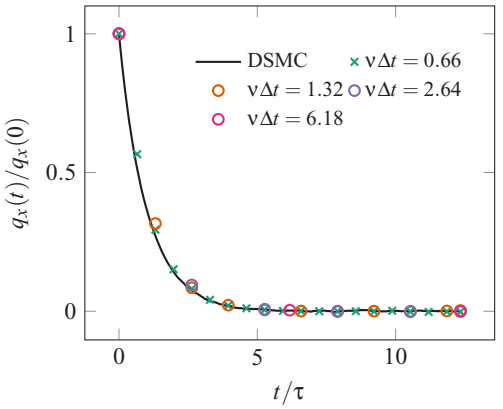

(b) Normalized heat flux

FIG. 2. Pressure tensor and heat flux relaxations with different time step sizes Δt using the ED-SP-BGK method with the linear approximation. The finely resolved DSMC results are provided as the reference. The time is normalized using the relaxation time τ.

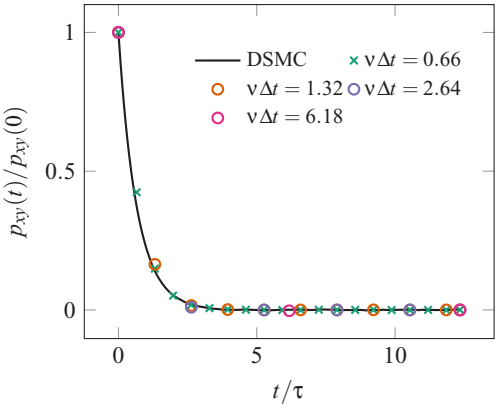

(a) Normalized shear stress

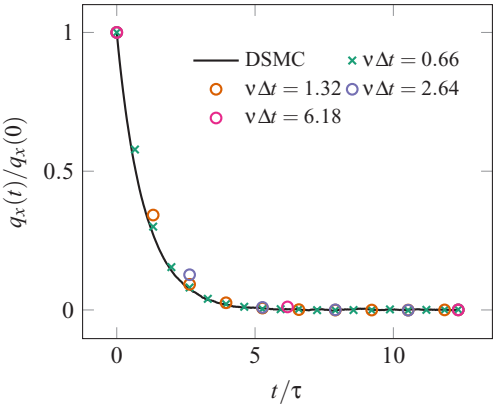

(b) Normalized heat flux

FIG. 3. Pressure tensor and heat flux relaxation with different time step sizes Δt using the ED-SP-BGK method with the exponential approximation. The finely resolved DSMC results are provided as the reference.

ED-SP-BGK. Therefore, an adaptive subcell method besides the time step size of $\Delta t_{\mathrm{DSMC}} = 2 \times 10^{-7}$ s was used to resolve the mean-free path and the mean collision time for the DSMC method. The ED-SP-BGK simulations were performed with the same time step as in the rarefied simulation. Thus, a factor of $\nu\Delta t \approx 3.5$ was obtained. As can be seen in Fig. 5, the ED-SP-BGK method achieves similar number density, mean velocity, and temperature with significantly coarser discretization. Both the linear and exponential approximations were tested, yielding negligible differences. For the next test cases, therefore, only the linear approximation was used. In this simulation, since time-accurate results at a certain physical time and not steady-state results are compared, relatively many particles per cell are needed with the stochastic methods (both DSMC and ED-SPBGK) to minimize noise. Nevertheless, in the continuum case, DSMC requires 10 times more particles than the ED-SP-BGK method to sufficiently resolve the mean-free path. Therefore, the single time step of the ED-SP-BGK method is already about eight times faster than DSMC. In addition, the time steps of $\Delta t_{\mathrm{ED-SPBGK}}/\Delta t_{\mathrm{DSMC}} = 150$ are very different, so to achieve the same physical time, DSMC needs about 1200 times the time of ED-SP-BGK.

C. Couette flow

The next test case is a steady planar Couette flow of argon, confined between the two parallel plates which move in opposite directions with the velocity $v_{\mathrm{wall}} = \pm 500$ m/s. The initial temperature of the gas as well as the wall temperature are $T = 273$ K leading to a supersonic Couette flow. The Couette flow was carried out in three different Knudsen number ranges. The conditions are shown in Table I. In the table, the reference time step is also given, for which the solution of the standard SP-BGK method becomes identical to the proposed ED-SP-BGK method. In order to investigate solely the influence of the time integration on the performance of the two methods, identical spatial interpolation was performed in both SP-BGK and ED-SP-BGK.

An important feature of wall-bounded gas flows is the gas-boundary interaction. In stochastic particle methods, the time and location where a particle hits the boundary are estimated using linear interpolation. This has been shown to reset the scheme back to the first order [32,33], close to the boundaries. Consistent high-order treatment of boundaries normally involves extensive modifications in the underlying stochastic process (e.g., see the walk on sphere scheme for the case of random walks [34,35]) Such treatments go beyond the scope

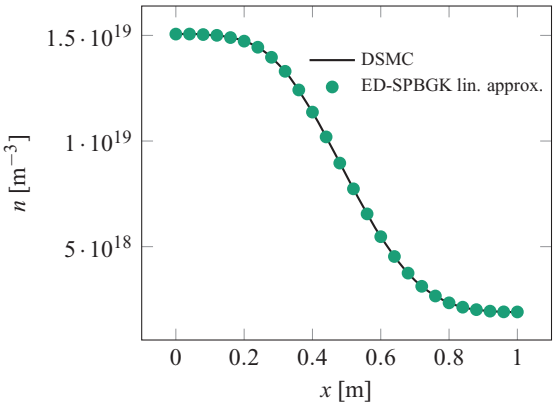

(a) Number density

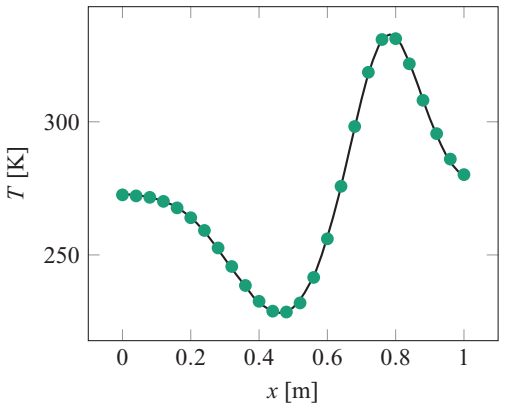

(b) Temperature

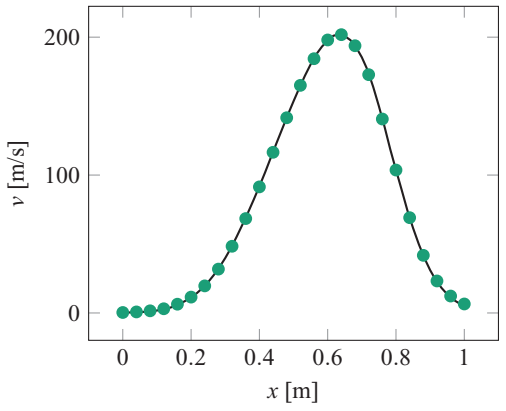

(c) Velocity

FIG. 4. Rarefied Sod shock tube test case. ED-SP-BGK, and reference DSMC results were computed using the same spatiotemporal resolution.

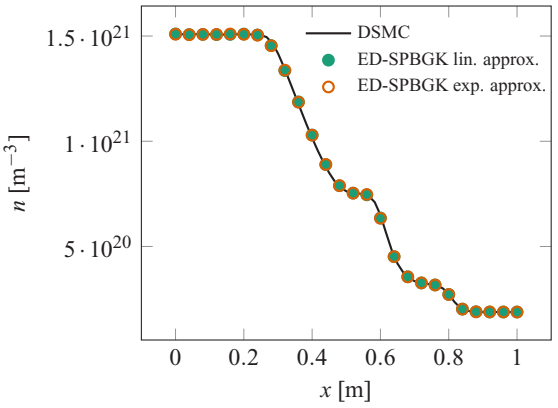

(a) Number density

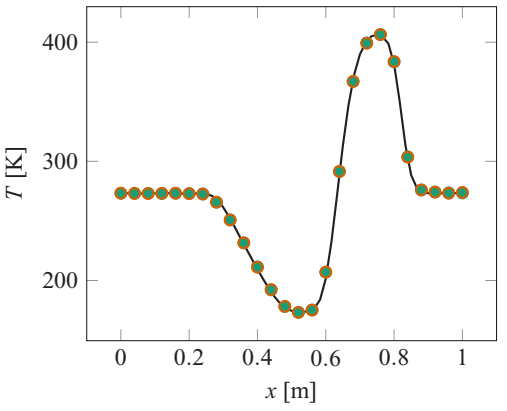

(b) Temperature

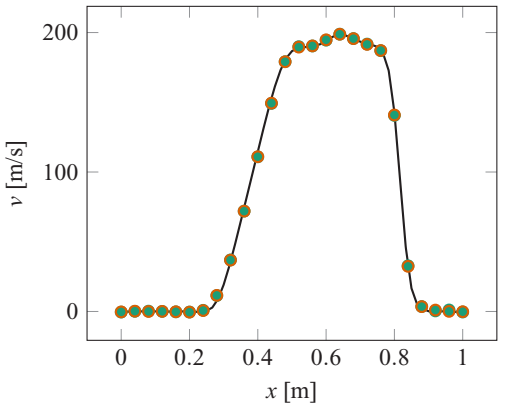

(c) Velocity

FIG. 5. Continuum Sod shock tube test case. ED-SP-BGK and reference DSMC results were computed, where much coarser resolution has been employed for ED-SP-BGK.

of this study, yet it should be noted that a certain reduction in the order of time integration will be observed in following scenarios where boundary interactions become dominant.

1. Kn=0.1

The first Couette flow is in the rarefied range with Kn = 0.1. Figure 6 shows results of ED-SP-BGK and SP-BGK with different time step sizes. For the coarsest case of $32\Delta t$, a factor of maximum $v\Delta t \approx 0.8$ is obtained in the simulation region. We observe that the ED-SP-BGK method achieves significantly better results compared to the SP-BGK method, even in the rarefied range where $v\Delta < t$. In Fig. 7 the velocity in the y direction v_y is depicted. Here both methods match the reference solution quite well for the different time step sizes.

2. Kn=0.01

In the transition regime with Kn = 0.01, the performance of the SP-BGK method becomes worse for larger time step

TABLE I. Start conditions of Couette flow simulations.

	No. computational cells	Number density [m^{-3}]	Kn	Δt_{ref} [s]
Case 1	25	1.37×10^{19}	0.1	1×10^{-5}
Case 2	100	1.37×10^{20}	0.01	5×10^{-6}
Case 3	500	1.37×10^{21}	0.001	6.25×10^{-7}

sizes as depicted in Fig. 8. The nondimensional time step reaches $\nu\Delta t \approx 2$ for the largest time step size of $16\Delta t$. The ED-SP-BGK method still shows good agreements with the reference solution. The time step is bounded by the CFL condition. The velocity plot depicted in Fig. 9 again shows good agreement for both methods.

3. Kn=0.001

The last test case enters the continuum range with Kn = 0.001. Here the required time step size to accurately resolve the solution becomes prohibitively small for the SP-BGK method, as shown in Fig. 10. We get $\nu\Delta t \approx 5$ corresponding to the time step size of $32\Delta t$, where again the ED-SP-BGK scheme performs reasonably well. For the velocity plots in Fig. 11, the picture is the same as before. Both methods can represent the velocity very well.

D. Poiseuille flow

A similar setup is employed in the Poiseuille flow, which consists once more an argon gas confined between two parallel plates in a distance of $L_y = 1$ m. The initial temperature of the gas as well as the wall temperature are $T = 273$ K. In this case, however, the walls do not move, but a constant volume force $\mathbf{F}$ acts on the gas and accelerates it. The diffuse reflection from the walls then leads to a characteristic velocity profile in the gas. In order to achieve second order with the force term as well, we use here the Strang splitting method [36]. Thus, after constructing $\hat{f}^*$ out of $\tilde{f}^*$ and before moving the particles, we add half the force to the velocities of the particles:

$$\mathbf{v}^{t_{1/2}} = \mathbf{v}^t + \frac{\Delta t}{2m}\mathbf{F}. \tag{58}$$

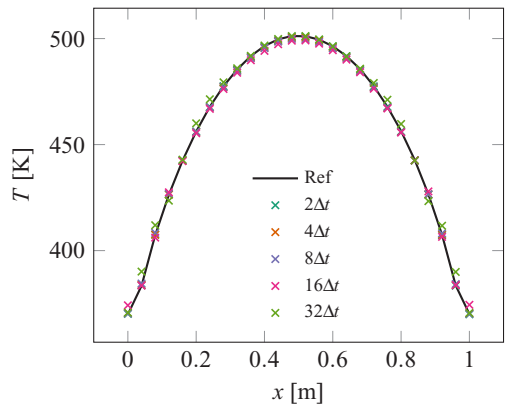

(a) ED-SPBGK

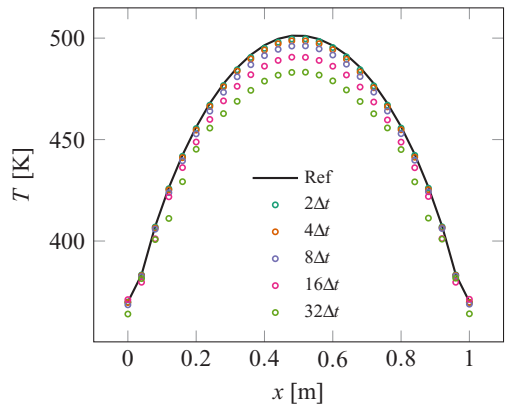

(b) SPBGK

FIG. 6. Comparison of temperature using ED-SP-BGK and SP-BGK as well as different time steps Δt for Couette flow with Kn = 0.1.

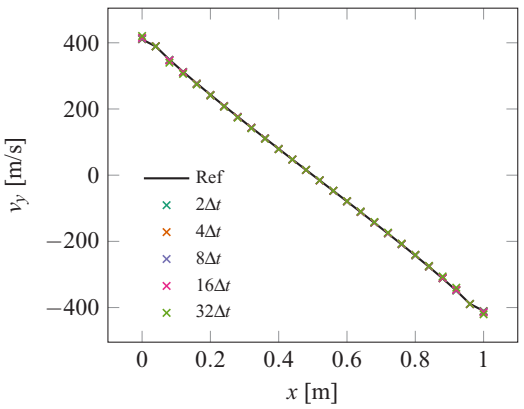

(a) ED-SPBGK

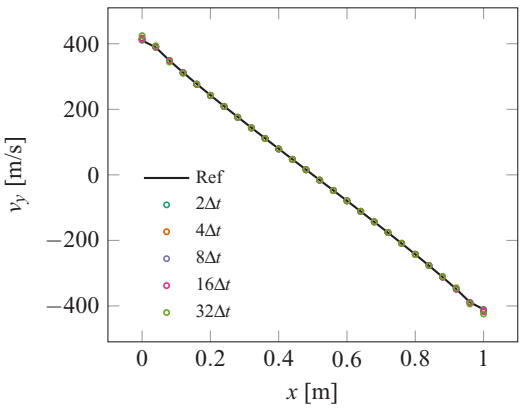

(b) SPBGK

FIG. 7. Comparison of velocity v_y using ED-SP-BGK and SP-BGK as well as different time steps Δt for Couette flow with Kn = 0.1.

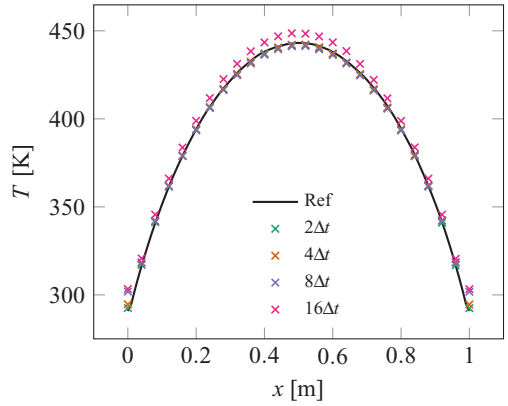

(a) ED-SPBGK

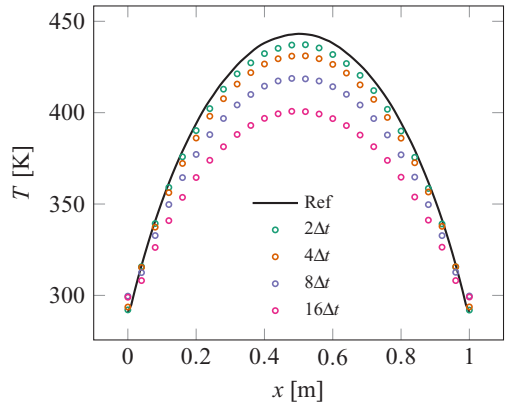

(b) SPBGK

FIG. 8. Comparison of temperature using ED-SP-BGK and SP-BGK as well as different time steps Δt for Couette flow with Kn $= 0.01$.

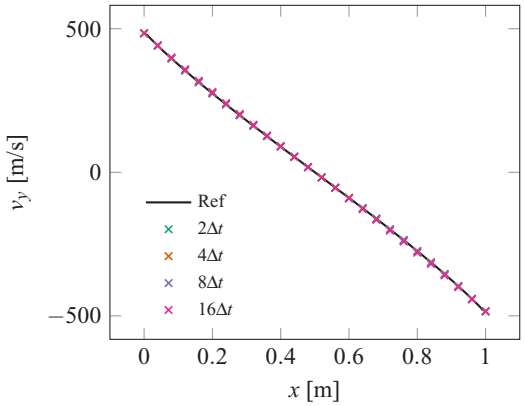

(a) ED-SPBGK

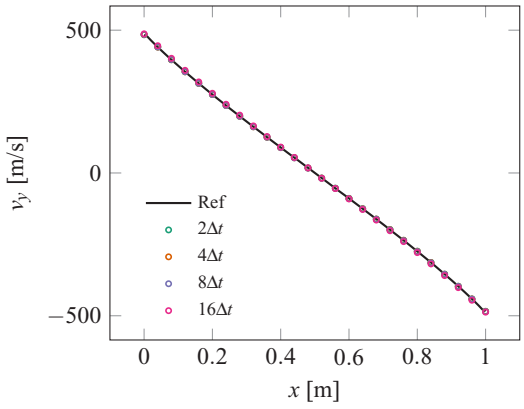

(b) SPBGK

FIG. 9. Comparison of velocity v_y using ED-SP-BGK and SP-BGK as well as different time steps Δt for Couette flow with Kn $= 0.01$.

Using these velocities, the particles are moved, and the other half of the force term is added afterwards in the same way to finalize the time step. The force term was chosen as $nF_x = 10^{-2}$ Pa/m, and again rarefied and continuum regime simulations were done.

1. Rarefied case

The first case uses a density of $n = 1.37 \times 10^{19}$ m^{-3} for a rarefied flow with a Knudsen number Kn ≈ 0.1. The flow is simulated with SP-BGK and ED-SP-BGK methods, with a fixed Courant-Friedrichs-Lewy number CFL ≈ 5, leading to different time steps for different cell numbers. The resulting relaxation factors are $\nu\Delta t = 0.08,\ 0.16,\ 0.33,\ 0.66,\ 1.63$ for, respectively, 200, 100, 50, 25, and 10 cells. The results are compared in Fig. 12 to a reference solution, obtained using DSMC on a 200 cells mesh. While, in this case, the SP-BGK method is already close to the reference with only 10 cells, the second-order nature of ED-SP-BGK allows it to better perform when the spatiotemporal resolution improves. The error convergence is shown in Fig. 13, where the results of each method are compared to the solutions obtained with the finest resolution, because no analytical solution is available in this case. As expected, the ED-SP-BGK method displays second order while SP-BGK converges only linearly. Only three different resolutions were used because ED-SP-BGK then levels out due to the stochastic error that would require many more simulation particles to be overcome. In this rarefied case, the calculation times of the DSMC and the ED-SPBGK are again in the same range as expected.

2. Continuum case

In the continuum case, a density of $n = 1.37 \times 10^{21}$ m^{-3} is used, which corresponds to a Knudsen number of Kn ≈ 0.001. In the continuum domain it is possible to formulate an analytical solution for the velocity profile [37]:

$$v_x = \frac{\rho F_x}{m}\frac{L_y y - y^2}{2\mu} \tag{59}$$

with the mass density ρ and the y position y. The solution of the ED-SP-BGK method and the SP-BGK method compared to the analytical solution are depicted in Fig. 14. Here a constant Courant-Friedrichs-Lewy condition of around CFL $= 0.35$ is used. This leads to the factors $\nu\Delta t = 0.6, 0.82, 1.2, 2.4$ for the number of cells 200, 150, 100, 50, correspondingly. As shown in Fig. 14, it is very clear that with the ED-SP-BGK method significantly fewer cells can be used

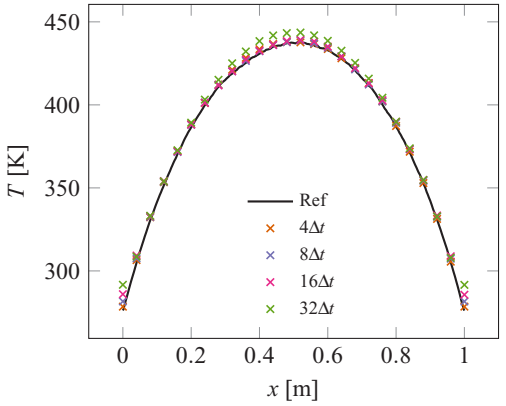

(a) ED-SPBGK

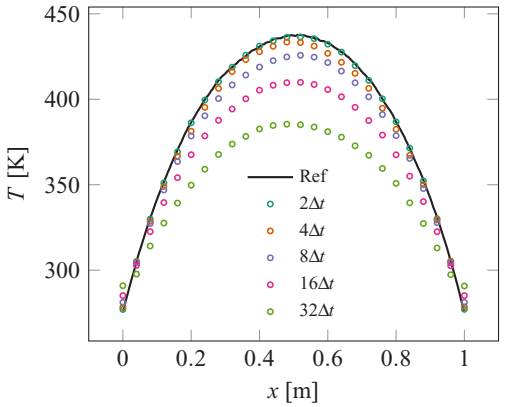

(b) SPBGK

FIG. 10. Comparison of temperature using ED-SP-BGK and SP-BGK as well as different time steps Δt for Couette flow with $\mathrm{Kn} = 0.001$.

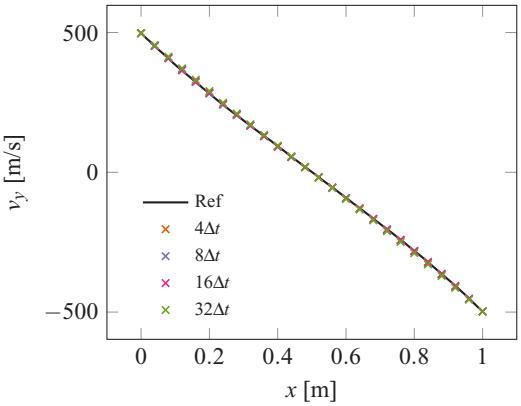

(a) ED-SPBGK

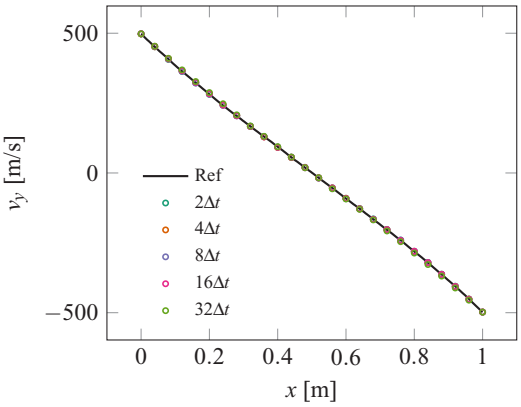

(b) SPBGK

FIG. 11. Comparison of velocity v_y using ED-SPBGK and SP-BGK as well as different time steps Δt for Couette flow with $\mathrm{Kn} = 0.001$.

at significantly larger time steps to obtain the analytical result than with the normal SP-BGK method. Furthermore, Fig. 15 shows the L^2 error of the two methods. One can see that ED-SP-BGK is second order whereas SP-BGK is first order. Due to the long calculation time, a DSMC calculation was not carried out here up to the steady state, but 1600 cells and a time step 10 times smaller than in ED-SPBGK with 150 cells were necessary in a test simulation to resolve the mean-free path and the mean collision time. Because of the smaller number of cells, about 20 times fewer particles were used in the ED-SPBGK simulation. Ultimately, to achieve the same physical end time, i.e. to reach steady state, DSMC needs about 30 times more computing time compared to the ED-SPBGK method. However, the DSMC method in PICLas is already heavily optimized in terms of computing time, whereas the ED-SPBGK is still in a developmental state, and no code optimization has yet been carried out. Here it is very clear how much coarser discretization can be used with the proposed ED-SPBGK method compared to the normal SPBGK method or DSMC. However, in this case, with 150 cells, significantly more cells are still needed than with the already mentioned DUGKS method, which requires significantly fewer cells for the same number of Knudsen cells [38]. The first tests with the exponential time integration proposed here for a DVM code have also shown that with this DVM implementation only 20 cells are necessary instead of 150 with particles. So this still seems to be a problem of the particle method itself. It is possible that the cell-based energy and momentum conservation algorithm in the particle method causes an additional error. In the future, other methods should be investigated that do not only perform energy and momentum conservation with the cell-based values and possibly further improve the discretization. Other methods for spatial interpolation should also be investigated in the future in order to further improve the spatial resolution.

IV. CONCLUSION

Particle methods comprise an attractive class of algorithms, which are typically employed for rarefied gas simulations. Despite their popularity and robustness, their numerical accuracy and convergence order hardly go beyond first order. Multiscale flow phenomena with realistic rarefaction regimes, however, require high-order schemes and thus entail fundamental improvements on numerical aspects of the stochastic particle methods. This study enhances SP-BGK schemes by introducing a consistent second-order treatment of the BGK relaxation, using the exponential differencing method. The structure of the devised ED-SP-BGK method allows for a

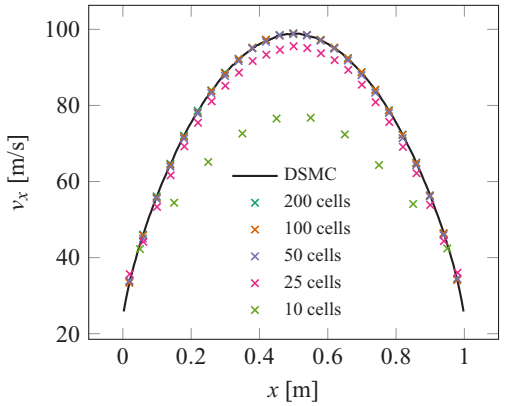

(a) ED-SP-BGK

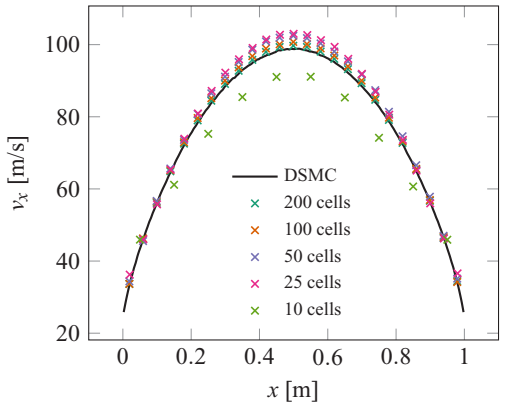

(b) SP-BGK

FIG. 12. Comparison of velocity v_x using ED-SP-BGK and SP-BGK as well as different resolutions for Poiseuille flow with Kn = 0.1.

straightforward implementation and minimal overhead with respect to the traditional SP-BGK method, as the particle weights remain nonnegative irrespective of the spatiotemporal scales. Besides correct asymptotic limits of the proposed ED-SP-BGK scheme in both free-molecular and continuum limits, its performance was investigated in a few standard settings covering a large variation of the Knudsen number. It is

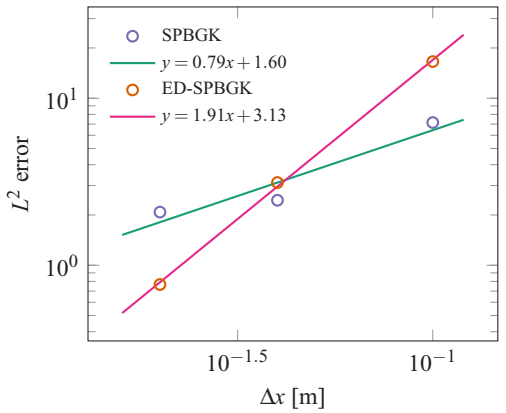

FIG. 13. Comparison of L^2 error using ED-SP-BGK and SP-BGK for Poiseuille flow with Kn = 0.1.

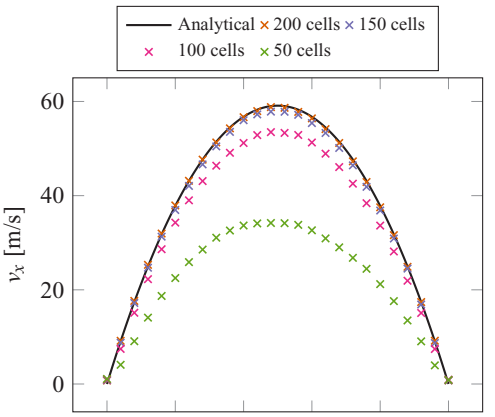

(a) ED-SP-BGK

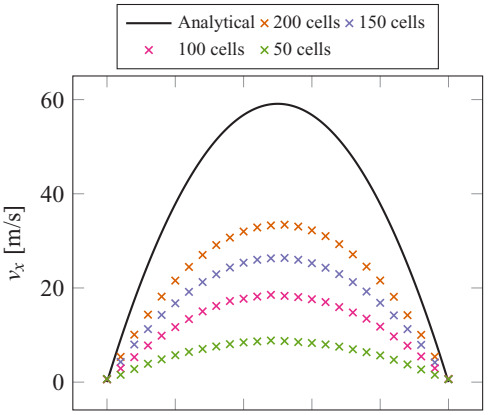

(b) SP-BGK

FIG. 14. Comparison of velocity v_x using ED-SP-BGK and SP-BGK as well as different resolutions for Poiseuille flow with Kn = 0.001.

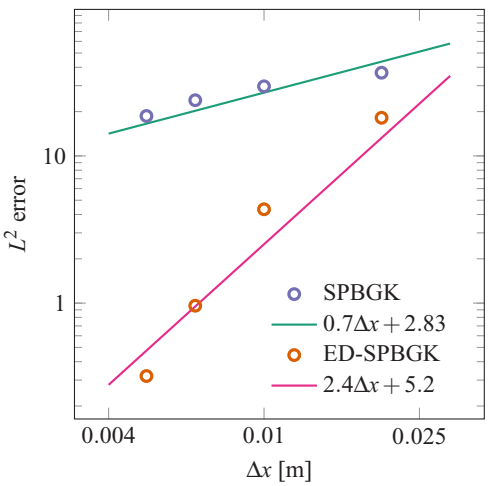

FIG. 15. Comparison of L^2 error using ED-SPBGK and SPBGK for Poiseuille flow with Kn = 0.001.

demonstrated that the devised scheme performs better than the SP-BGK method in all considered scenarios including both rarefied and continuum regimes. Extension of the scheme for more complex gas flow scenarios besides improved treatment of the boundary conditions will be pursued in the follow-up studies.

ACKNOWLEDGMENT

This project has received funding from the European Research Council (ERC) under the European Union's Horizon 2020 research and innovation program (Grant Agreement No. 899981 MEDUSA).

APPENDIX: TIME-DEPENDENT DISTRIBUTION FUNCTION IN THE CONTINUUM LIMIT

This analysis is based on the procedure given by Guo *et al.* [7]. Let us consider Eq. (27),

$$f(\mathbf{v},\mathbf{x}+\mathbf{v}\Delta t,t+\Delta t) = \frac{1-e^{-\nu\Delta t}}{\nu\Delta t}\tilde{f}^{*}(\mathbf{v},\mathbf{x}+\mathbf{v}\Delta t,t+\Delta t) + \left(1-\frac{1-e^{-\nu\Delta t}}{\nu\Delta t}\right)f^{M}(\mathbf{v},\mathbf{x}+\mathbf{v}\Delta t,t+\Delta t), \quad \text{(A1)}$$

where it is assumed $f^{t}=f^{M}$. In addition, state $(\mathbf{v},\mathbf{x}+\mathbf{v}\Delta t,t+\Delta t)$ is abbreviated as $(t+\Delta t)$ and state $(\mathbf{v},\mathbf{x},t)$ as (t). It is known that $\tilde{f}^{*}(\mathbf{v},\mathbf{x}+\mathbf{v}\Delta t,t+\Delta t)$ results from the movement of the particles along the trajectories of $\hat{f}^{*}(\mathbf{v},\mathbf{x},t)$, which corresponds to the advection step $\tilde{f}^{*}(\mathbf{v},\mathbf{x}+\mathbf{v}\Delta t,t+\Delta t)=\hat{f}^{*}(\mathbf{v},\mathbf{x},t)-\mathbf{v}\Delta t\nabla\hat{f}^{*}(\mathbf{v},\mathbf{x},t)$. Substituting this into (A1) and using (27) yields

$$f\ (t+\Delta t) = \frac{1-e^{-\nu\Delta t}}{\nu\Delta t}\left[\frac{\nu\Delta t e^{-\nu\Delta t}}{1-e^{-\nu\Delta t}}[f(t)-\mathbf{v}\Delta t\nabla f(t)] + \left(1-\frac{\nu\Delta t e^{-\nu\Delta t}}{1-e^{-\nu\Delta t}}\right)[f^{M}(t)-\mathbf{v}\Delta t\nabla f^{M}(t)]\right] + \left(1-\frac{1-e^{-\nu\Delta t}}{\nu\Delta t}\right)f^{M}(t+\Delta t). \quad \text{(A2)}$$

Let $f^{M}(t+\Delta t)\approx f^{M}(t)+\Delta t\partial_t f^{M}(t)$, which is justified in the continuum limit as discussed in Guo *et al.* [7], and suppose that $f(t)$ in the continuum limit can be approximated by the Chapman-Enskog expansion

$$f(t)\approx f^{M}(t)-\tau D_t f^{M}(t)+O\left(D_t^2\right) \quad \text{(A3)}$$

with $D_t=(\partial_t+\mathbf{v}\nabla)$; then Eq. (A2) leads to

$$\begin{aligned} f(t+\Delta t) = {} & e^{-\nu\Delta t}[f^{M}(t)-\tau D_t f^{M}(t)] + \left(\frac{1-e^{-\nu\Delta t}}{\nu\Delta t}-e^{-\nu\Delta t}\right)f^{M}(t) \\ & + \left(1-\frac{e^{-\nu\Delta t}}{\nu\Delta t}\right)[f^{M}(t)+\Delta t\partial_t f^{M}(t)] \\ & - \mathbf{v}\Delta t\left[e^{-\nu\Delta t}\nabla f^{M}(t)+\left(\frac{1-e^{-\nu\Delta t}}{\nu\Delta t}-e^{-\nu\Delta t}\right)\times\nabla f^{M}(t)\right]+O(\partial^2), \end{aligned} \quad \text{(A4)}$$

Further rearrangements of the prefactors yields

$$f(t+\Delta t)=f^{M}(t)-\tau D_t f^{M}(t)+\Delta t\partial_t f^{M}(t)+O(\partial^2), \quad \text{(A5)}$$

which is the time-dependent Chapman-Enskog Navier-Stokes distribution [7].

[1] G. A. Bird, *Molecular Gas Dynamics and the Direct Simulation of Gas Flows* (Oxford University Press, New York, 1994).
[2] D. Hash and H. Hassan, in *33rd Aerospace Sciences Meeting and Exhibit* (AIAA, Reston, VA, 1995), Paper No. AIAA-95-0410.
[3] H. Carlson, R. Roveda, I. Boyd, and G. Candler, in *42nd AIAA Aerospace Sciences Meeting and Exhibit* (AIAA, Reston, VA, 2004), p. 1180.
[4] L. Mieussens, Math. Models Methods Appl. Sci. **10**, 1121 (2000).
[5] K. Xu and J.-C. Huang, J. Comput. Phys. **229**, 7747 (2010).
[6] S. Chen and K. Xu, J. Comput. Phys. **288**, 52 (2015).
[7] Z. Guo, K. Xu, and R. Wang, Phys. Rev. E **88**, 033305 (2013).
[8] C. Liu, Y. Zhu, and K. Xu, J. Comput. Phys. **401**, 108977 (2020).
[9] M. Pfeiffer, Phys. Fluids **30**, 106106 (2018).
[10] J. Zhang, B. John, M. Pfeiffer, F. Fei, and D. Wen, Adv. Aerodyn. **1**, 1 (2019).
[11] M. Pfeiffer, A. Mirza, and P. Nizenkov, Phys. Fluids **31**, 073601 (2019).
[12] M. H. Gorji and P. Jenny, J. Comput. Phys. **262**, 325 (2014).
[13] M. H. Gorji and M. Torrilhon, J. Comput. Phys. **430**, 110034 (2021).
[14] J. Mathiaud and L. Mieussens, J. Stat. Phys. **162**, 397 (2016).
[15] M. Gallis and J. Torczynski, Phys. Fluids **23**, 030601 (2011).
[16] M. Gallis and J. Torczynski, The application of the BGK model in particle simulations, in *34th Thermophysics Conference* (AIAA, Reston, VA, 2000), pp. 2000–2360, doi: 10.2514/6.2000-2360.
[17] F. Fei, H. Liu, Z. Liu, and J. Zhang, AIAA J. **58**, 2596 (2020).
[18] M. H. Gorji, M. Torrilhon, and P. Jenny, J. Fluid Mech. **680**, 574 (2011).
[19] S. V. Bogomolov, Math. Models Comput. Simul. **1**, 739 (2009).
[20] P. L. Bhatnagar, E. P. Gross, and M. Krook, Phys. Rev. **94**, 511 (1954).
[21] W. G. Vincenti and C. H. Kruger, *Introduction to Physical Gas Dynamics* (Wiley, New York, 1965).
[22] L. H. Holway Jr, Phys. Fluids **9**, 1658 (1966).
[23] E. Shakhov, Fluid Dyn. **3**, 95 (1968).
[24] H. Struchtrup, Continuum Mech. Thermodyn. **9**, 23 (1997).
[25] F. Fei, J. Zhang, J. Li, and Z. Liu, J. Comput. Phys. **400**, 108972 (2020).

[26] F. Fei, Y. Ma, J. Wu, and J. Zhang, Adv. Aerodyn. **3**, 18 (2021).
[27] S. M. Cox and P. C. Matthews, J. Comput. Phys. **176**, 430 (2002).
[28] C.-D. Munz, M. Auweter-Kurtz, S. Fasoulas, A. Mirza, P. Ortwein, M. Pfeiffer, and T. Stindl, C. R. Mec. **342**, 662 (2014).
[29] S. Fasoulas, C.-D. Munz, M. Pfeiffer, J. Beyer, T. Binder, S. Copplestone, A. Mirza, P. Nizenkov, P. Ortwein, and W. Reschke, Phys. Fluids **31**, 072006 (2019).
[30] J. Burt and I. Boyd, in *44th AIAA Aerospace Sciences Meeting and Exhibit* (AIAA, Reston, VA, 2006), p. 989.
[31] H. Struchtrup and M. Torrilhon, Phys. Fluids **15**, 2668 (2003).
[32] D. J. Higham, X. Mao, M. Roj, Q. Song, and G. Yin, SIAM/ASA J. Uncertainty Quantif. **1**, 2 (2013).
[33] E. Gobet and S. Menozzi, Stochast. Proc. Appl. **112**, 201 (2004).
[34] K. K. Sabelfeld, Monte Carlo Methods Appl. **22**, 265 (2016).
[35] M. Muller, Ann. Math. Stat. **26**, 537 (1955).
[36] G. Strang, SIAM J. Numer. Anal. **5**, 506 (1968).
[37] R. Myong, Phys. Fluids **23**, 012002 (2011).
[38] P. Wang, M. T. Ho, L. Wu, Z. Guo, and Y. Zhang, Comput. Fluids **161**, 33 (2018).